Journal of Biomedical Optics

BiomedicalOptics.SPIEDigitalLibrary.org

Increasing depth penetration in biological tissue imaging using 808-nm excited $Nd^{3+}/Yb^{3+}/Er^{3+}$-doped upconverting nanoparticles

Hugo Söderlund
Monirehalsadat Mousavi
Haichun Liu
Stefan Andersson-Engels

SPIE.

Increasing depth penetration in biological tissue imaging using 808-nm excited $Nd^{3+}/Yb^{3+}/Er^{3+}$-doped upconverting nanoparticles

Hugo Söderlund,[†] Monirehalsadat Mousavi,[†] Haichun Liu, and Stefan Andersson-Engels[*]
Lund University, Biophotonics Group, Department of Physics, P.O. Box 118, SE-22100 Lund, Sweden

Abstract. Ytterbium (Yb^{3+})-sensitized upconverting nanoparticles (UCNPs) are excited at 975 nm causing relatively high absorption in tissue. A new type of UCNPs with neodymium (Nd^{3+}) and Yb^{3+} codoping is excitable at a 808-nm wavelength. At this wavelength, the tissue absorption is lower. Here we quantify, both experimentally and theoretically, to what extent Nd^{3+}-doped UCNPs will provide an increased signal at larger depths in tissue compared to conventional 975-nm excited UCNPs. [DOI: 10.1117/1.JBO.20.8.086008]

Keywords: upconverting nanoparticles; tissue optics; deep tissue imaging.

Paper 150191RR received Mar. 23, 2015; accepted for publication Jul. 15, 2015; published online Aug. 13, 2015.

1 Introduction

Upconverting nanoparticles (UCNPs) are becoming highly interesting in the field of biophotonics due to their upconverting properties supporting minimal autofluorescense background under near-infrared excitation.[1] Other beneficial aspects of UCNPs include high-imaging resolution and relatively large penetration depth in tissues of both excitation and emission light, as well as the absence of photobleaching and photoblinking.[2] However, there are still challenges with UCNPs, such as low quantum yield compared to traditional downconverting fluorophores and a nonoptimal attenuation of the excitation light in tissue.[2] Thus it is beneficial to improve these aspects of the UCNPs to increase overall efficiency.

In most UCNPs, there is a sensitizer and an activator, where the sensitizer absorbs the excitation photons and transfers the energy to the activator in order to achieve upconversion. As of today, ytterbium (Yb^{3+})-sensitized and Tm^{3+}- or Er^{3+}- activated $NaYF_4$ UCNPs are promising contrast agents for bioimaging and are being intensively studied.[2–5] They both exhibit several strong luminescence emission bands. In tissue imaging, the emission bands at 800 and 650 nm are preferentially used as they are within the tissue optical window enabling good light penetration in tissue. Both these bands can be excited with 975-nm light due to the Yb^{3+} absorption. These wavelengths all match the optical window for biological tissue, well known to be between 600 and 1300 nm.[6] While the Yb^{3+}/Tm^{3+} $NaYF_4$ UCNPs (Yb:UCNPs) operate within this region, Yb^{3+} cannot be considered as an optimal sensitizer for deep tissue imaging due to the increased absorption of light in tissue due to water within the tissue optical window around 975 nm.[7] Recently, Nd^{3+}/Yb^{3+}-cosensitized and Er^{3+}-activated $NaYF_4$ UCNPs (Nd:UCNPs) have been introduced with an excitation wavelength at 808 nm and emission at 650 nm.[8] The motivation for the neodymium (Nd^{3+}) codoping is to provide better light penetration of the excitation light and provides possibilities to excite the UCNPs deeper into tissue. The water absorption is greatly reduced at the excitation wavelength of 808 nm as compared to at the excitation wavelength of 975 nm which is used for the conventionally employed UCNPs.[7] Since the upconversion process requires two or more excitation photons,[9] it should be more essential to minimize the attenuation of the excitation than the emission light in order to optimize the strength of the detected signal. Thus, by using an excitation wavelength with reduced absorption in tissue, it should be possible to increase the signal from deep locations in tissue.

The Nd:UCNPs allow Nd^{3+} to absorb the incoming photons and transfer the energy to the second sensitizer, Yb^{3+}, which subsequently transfers the energy to the activator in order to achieve upconversion.[8] The energy transfer efficiency between the Nd^{3+} and Yb^{3+} ions has been reported to be as high as 70%.[10] Meanwhile, Nd^{3+} has a larger absorption cross-section at 808 nm compared to that of Yb^{3+} at 975 nm. Furthermore, by using Nd:UCNPs in a core-shell structure, quenching of the UC emission due to unwanted energy transfer from the activator to Nd^{3+} ions is reduced, resulting in an optimal upconversion efficiency comparable to that of the Yb:UCNPs.[8] Most interestingly, the excitation wavelength at 808 nm will have a greatly reduced water absorption compared to that at 975 nm (0.02 cm^{-1} compared to 0.46 cm^{-1} for 100% water).[11]

In addition to reducing imaging depth, there have also been several reports stating that 975-nm excited UCNPs cause overheating due to the relatively high absorption by water for this wavelength.[2,10,12,13] Nd:UCNPs will drastically reduce any heating due to the reduced water absorption at 808 nm compared to at 975 nm.[8] The present report is intended to quantify the advantages in tissue penetration for Nd:UCNPs compared to that of Yb:UCNPs. Here, we thoroughly investigate the imaging depth advantages of $NaYF_4:Yb^{3+}/Er^{3+}/Nd^{3+}$ UCNPs compared to using $NaYF_4:Yb^{3+}/Tm^{3+}$ UCNPs by performing

*Address all correspondence to: Stefan Andersson-Engels, E-mail: stefan.andersson-engels@fysik.lth.se

†Authors contributed equally on this paper.

1083-3668/2016/$25.00 © 2016 SPIE

measurements in tissue phantoms in addition to Monte Carlo (MC) simulations for varying tissue compositions.

2 Experiment

2.1 *Materials*

The core-shell UCNPs used in the study were synthesized in-house. They are characterized in detail elsewhere.[14] The measurements conducted for this report were performed in tissue phantoms, containing 3% bovine blood, 3% intralipid-20%, and the remaining 94% tap water. The blood was purchased at the local supermarket in a frozen container and was stored in the refrigerator prior to the measurements. The blood was used within a week after purchase. The intralipid was of the brand Fresenius Kabi and contained intralipid 200 mg/ml. It was stored in the refrigerator in sealed containers before use. The water used in the tissue phantom was regular tap water. A cylindrical container made of glass with a diameter of 140 mm was used for the tissue phantom. The measurements were performed in transillumination geometry, as seen in Fig. 1. The thickness of the tissue phantom was 18 mm. Diode lasers (Thorlabs L808P1WJ for the 808-nm laser and Thorlabs L975P1WJ for the 975-nm laser) were used for excitation. The diode lasers were powered and temperature controlled by Thorlabs LDC 220 C and Thorlabs TED 200 C, respectively. The laser light was coupled into a 400 μm optical fiber and guided to the tissue phantom. The distal end of the optical fiber was imaged on the bottom surface of the tissue phantom by a 2.0 cm focal length lens to obtain a top-hat profile of the illumination spot. The diameter of the illumination spot was 5.0 and 7.0 mm for 808 and 975 nm, respectively. A bandpass filter (Omega Optical, NC 146753 Z800/40X for the 808-nm laser and 712M000040 BP-0975-056 for the 975-nm laser) was placed in front of the collimation lens in order to remove unwanted sidelobes of the laser light. The two samples containing the Nd:UCNPs and the Yb:UCNPs particles, respectively, were prepared by adding UCNPs into approximately 15 μl epoxy glue to create 3-mm diameter spherical samples. These UCNPs-containing glue-samples were cured on 0.148-mm transparent fishing thread

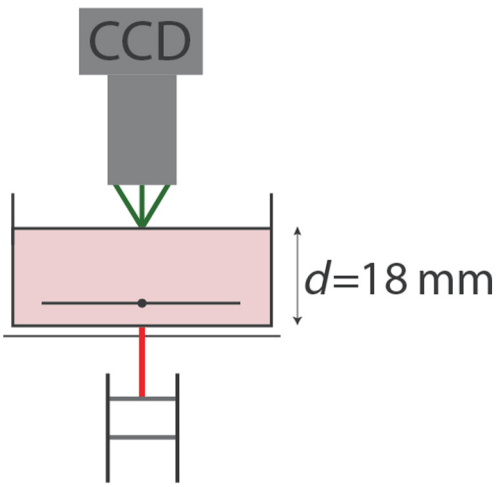

Fig. 1 Instrumental setup for the transillumination measurements. From bottom to top, fiber-coupled excitation laser (808 or 975 nm), collimation lens with bandpass filter, glass container with 18-mm thick tissue phantom, containing an upconverting nanoparticle (UCNP) inclusion, objective lens, filter tube, and camera.

and later attached to a custom-made metal holder, attached to a translator stage, allowing for positioning the UCNPs at different depths with a resolution of 20 μm. Above the container, the emitted light was collected by a lens (25-mm focal length and $f/0.95$, Xenon, Schneider-Kreuznach, Germany) connected to a filter tube which, in turn, was attached to an air-cooled CCD camera (Andor iXon$_+$, Belfast, Ireland). The filter tube used two achromatic doublet $f = 75$-mm lenses (Thorlab, ARC: 650 to 1050 nm) to create parallel light through the filters, in order to effectively block out unwanted light while transmitting the emission light.[15,16] For the Nd:UCNPs 650-nm emission, the filters, SP OD4—750 nm (Edmund Optics), BP 650 nm × 50 nm OD4 (Edmund Optics), and RED-50S (Chroma), were used to clean the emission while for the Yb:UCNPs 800-nm emission, the 900-nm short pass filter (Omega Optical, BSP 156613) and two 800 nm (Omega Optical, BP50 156612) were employed. These filters ensured that only the emission light from the selected bands contributed to the recorded signal.

2.2 *Methods*

For a comparison of two different UCNPs, it is necessary to ensure they both operate in an unsaturated regime in all measurements in order to enable general conclusions from the comparison. The aim of the first measurements was to find an excitation intensity regime in which the particles were not saturated. When a nonsaturated region was found, depth measurements were performed with the corresponding nonsaturated excitation intensity. Here, the excitation intensity was kept constant while the depth of the sample into the tissue phantom was increased in a stepwise manner. An image was taken for each step, with a corresponding background image without the UCNP sphere subtracted.

2.2.1 *Power dependence*

A power dependence measurement was performed at a depth of 3.0 mm into the phantom, the same as the initial depth for the following depth measurements. Here, zero depth is established when the sample is just in contact with the bottom of the container. The power was varied from 50 to 140 mW with a factor of 1.1 between each step for the Nd:UCNPs. The spotsize at the surface of the phantom was 5.0 mm in diameter. For the Yb:UCNPs, the power was varied from 20 to 73 mW with a factor of 1.1 between each step with a spotsize of 7.0 mm in diameter. The exposure time was set to 9.9 s for each image for both sample measurements; an electron-multiplying (EM) gain of 10 for the Nd:UCNPs and an EM gain of 100 for the Yb:UCNPs were employed. A binning of 8 × 8 pixels was used for both samples. A final image without any UCNP sample was recorded in order to effectively subtract the background from each recorded image. The images were analyzed in MATLAB where the value of each pixel was summed up for each image and plotted as a function of excitation intensity (mW/cm^2).

2.2.2 *Depth measurements*

Depth measurements were conducted under nonsaturation excitation conditions, as confirmed by the power dependence measurements. The samples were positioned at a starting depth of 3.0 mm into the 18-mm deep tissue phantom, and the depth was increased stepwise with 0.5 mm per step until a total depth of 10 mm was reached. The zero depth was as defined above as

when the sample was just in contact with the bottom of the glass container. The excitation power was 70 mW for both lasers, corresponding to an intensity of 407 and 207 mW/cm^2 for the 808- and 975-nm lasers, respectively. The spotsize was again 5.0 and 7.0 mm in diameter for the 808- and 975-nm lasers, respectively. For each depth position, an image was recorded. Directly after completing the measurements at all depths, a sample-free image was recorded in order to enable subtraction of the background from each recorded image. The same setup as in the power dependence measurements was used. Every image was recorded using an acquisition time of 9.9 s. A binning of 8×8 pixels was employed and the EM gain was set to 300 at the camera for all recordings. The images were analyzed in MATLAB and a square of 10×10 pixels was summed up, with the largest value pixel in the center of the square.

2.2.3 *Monte Carlo simulations*

To investigate how the potential signal gain for the Nd:UCNPs versus the Yb:UCNPs was influenced by the tissue composition, MC simulations of the transport of excitation and emission light in tissue were employed. The MC code used for this purpose was CUDAMCML.[17] The absorption coefficients for the chromophores used in the measurements, i.e., blood, fat, water, and melanin, were extracted from relevant publications.[7,18–20] The wavelengths of interest were 975, 808, and 650 nm, which include the excitation and emission wavelengths for both UCNPs employed.

The first simulation was performed aiming for the same optical properties as the tissue phantom in the experimental measurements, i.e., a phantom with a volume fraction of 3% blood, 3% intralipid (20% stock solution), and 94% water. The blood was assumed to be 75% oxygenated. For the simulation, the absorption properties of 20% intralipid stock solution were considered as those from 20% pure fat and 80% water. The reduced scattering was assumed to only depend on intralipid, and the values were obtained according to the equation from Aernouts et al.:[21]

$$\mu_s' = -76.7 + 1.71 \cdot 10^5 \cdot \lambda^{-0.957},$$

where λ is the wavelength (nm) and μ_s' is the reduced scattering coefficient [cm^{-1}]. The g-factor was set to 0.85. This resulted in the following optical properties: μ_a (650 nm) = 0.20 cm^{-1}, μ_a (800nm)=0.15cm^{-1}, μ_a (975nm)=0.60cm^{-1}, μ_s (650nm)= 54cm^{-1}, μ_s (800 nm) = 41 cm^{-1}, and μ_a (975 nm) = 32 cm^{-1}. In the simulations, 50 million photon packets were injected into the 18-mm thick tissue. One simulation was conducted for the excitation wavelength and one for the emission wavelength. The light was injected from opposite sides in the two simulations to simulate a transillumination measurement. This resulted in two fluence distributions in the tissue. A Jacobian, describing the probabilities for generating a signal at various positions in the tissue, was calculated as the excitation fluence squared times the emission fluence.

Next, the fat volume fraction was varied from 5% to 30% in the simulations while keeping the blood volume fraction constant at 3%, leaving the water volume fraction to vary from 92% to 67%. The scattering was assumed to be constant in these simulations and the same as above. The results were presented as the ratio of the signals simulated for the two types of UCNPs.

Another simulation included a variation of blood content in the tissue. In this simulation, the volume fraction of blood was gradually increased from 1% to 10% in steps of 0.5%. Here, a constant fat volume fraction of 5% was used and the water volume fraction varied from 94% to 85%. Again, the scattering was kept constant with values as above.

Finally, in order to simulate a realistic *in vivo* measurement, a thin layer of melanin was added at the tissue surface to simulate skin. The layer was 0.1-mm thick and had a varying melanin volume fraction of 1% to 45%, with a step-size of 1% and a constant fat concentration of 5%. In the simulations, the thin melanin layer contained no blood chromophores, and the remaining volume fraction was water. Below the 0.1-mm thick skin layer, the tissue contained 3% blood (75% oxygenation), 5% lipid, and 92% water. The entire tissue had constant scattering properties equal to previous simulations.

3 Results and Discussion

The results of the slope efficiency measurements of emission signal versus excitation intensity for the samples at a depth of 3.0 mm are shown in Fig. 2. This clearly shows a slope efficiency of 2.0 for both types of UCNPs, meaning the excitation relies on two photons and thus the UCNPs operate in a nonsaturated regime. Such dependence is expected for these UCNPs,[1] and secures that all measurements are conducted at low enough intensities such that no saturation takes place. As these measurements are conducted at the position closest to the excitation source in the following measurements, this ensures that all measurements were in the nonsaturated excitation regime and thus allowed straightforward comparisons. In addition, the graph shows that the excitation intensities differ for the two UCNPs samples. Data, not published here, suggest that the Yb:UCNPs sample used saturated at lower power densities than the Nd:UCNPs studied. Thus, we conducted the measurements at different intensities by using two beam size diameters, 5.0 and 7.0 mm. The difference in excitation intensities between the samples is not of primary interest in this study as we have not optimized the samples for efficiency. The particles may have different quantum yields as this is strongly dependent on the synthesis and neither is fully optimized nor measured for these particles. The concentration of the UCNPs may also vary between the two samples as this was difficult to control at the preparation. In Fig. 3, the signal as a function of sample depth is plotted for the two types of UCNPs. The signals are plotted both in linear and semilogarithmic scales to clearly visualize the gain in signal for the Nd:UCNPs. Under the used conditions, the UCNPs had an equal signal at 3.0-mm depth (not shown). In the figure, the signals are instead normalized to a value of 1 at a 3.0-mm depth to clearly illustrate the variation of signals with depth for the two types of UCNPs. The comparison of the two different particle signals as a function of depth yields significant improvement in the emission signal intensity for the Nd codoped particles.

The Nd:UCNPs showed a gain of about 7 times as compared to the Yb:UCNPs at a depth of 10 mm in the tissue phantom.

Figure 4 presents one set of MC simulations for the excitation and emission light. The probability map for detecting the emitted light is simulated in a reverse-path strategy.[22] A homogeneous sample of 18-mm thickness is studied in the simulations. The Jacobian generated from these simulations is also presented. This shows that most of the signals are generated close to the source. This can be understood as two excitation

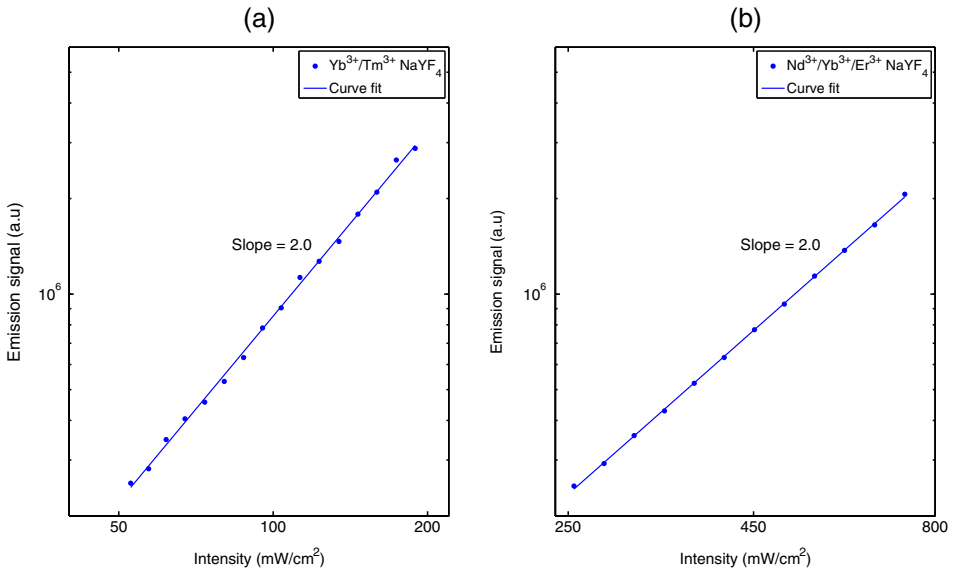

Fig. 2 Power dependence illustrated in a log–log plot of (a) $NaYF_4$:Yb^{3+}/Tm^{3+} and (b) $NaYF_4$:$Nd^{3+}/Yb^{3+}/Er^{3+}$. The intensity refers to excitation intensity at the surface of phantom.

photons are required per event, while only one emission photon is emitted. Thus, the attenuation of the excitation light is becoming dominant over the attenuation of the emission light, and the Jacobian will be clearly asymmetric. This shape suggests that it is more efficient to optimize the measured signal by reducing the attenuation of the excitation than the emission light. In Fig. 5, the experimentally measured signals from a sample at various depths in the tissue phantom are plotted together with MC results. The signal was again normalized to the value of 1.0 for a depth of 3.0 mm to enable a direct comparison on the relative slope of the MC modeled curve with experimental data. The comparison illustrates a good agreement between measurement and simulations. These modeled results deviate less than 20% for any measured data point. This is as good as one can expect with the values of the optical properties as taken from literatur with the samples being extended to 3.0 mm in diameter. MC simulations are known to provide accurate results and the CUDAMCML code has been benchmarked previously.[17]

Encouraged by the good agreement for the results of MC simulations, modeled results of the gain in signal by using Nd:UCNPs are presented for different optical properties in Fig. 6. The gain ratios, i.e., the ratios of the signals for the Nd:UCNPs and the Yb:UCNPs, are illustrated as a function of position in tissue and tissue composition. A gain ratio above the value 1 means that the Nd:UCNPs provide a stronger signal than the Yb:UCNPs—a signal gain, only due to the effect of less attenuation in the tissue. Gain values below the value 1 mean

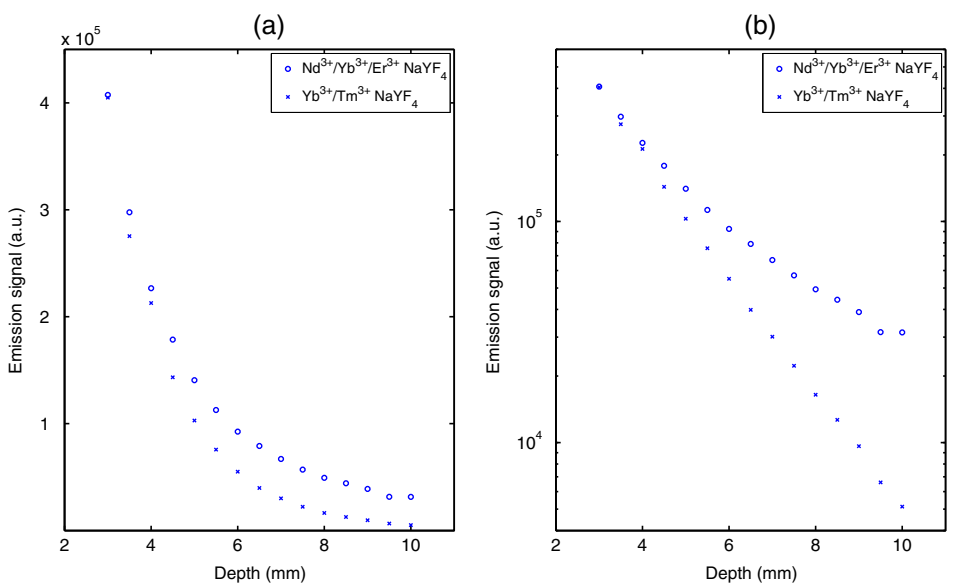

Fig. 3 Depth measurements of Yb^{3+}/Tm^{3+} and $Nd^{3+}/Yb^{3+}/Er^{3+}$: (a) a linear scale, and (b) a plot in semilogarithmic scale.

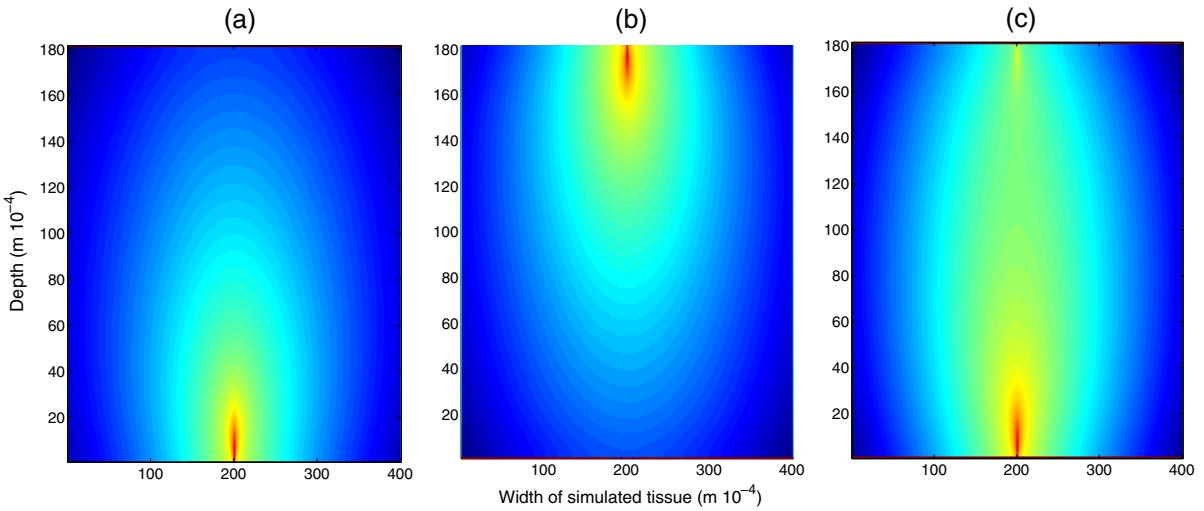

Fig. 4 An MCML simulation showing (a) the excitation fluence distribution in the tissue, (b) a probability map for detecting the emitted light as a function of position, and (c) the Jacobian of the excitation fluence distribution squared times the emission fluence distribution. The Jacobian represents a value of the detected signal strength at the detector for different localizations of the UCNP-sample within the tissue.

a signal loss, i.e., a lower signal for the Nd:UCNPs than for the the Yb:UCNPs, and are achieved for regions close to the source where the attenuation of the emitted light dominates the total light attenuation in tissue.

The lipid simulation shows that varying the lipid fraction has little impact on signal gain. The blood simulations show that for larger amounts of blood, the Nd:UCNPs have less gain compared to low blood volumes. For the simulations containing a thin melanin layer, it is shown that the gain for the Nd:UCNPs is higher for low quantities of melanin in the tissue.

For certain compositions of tissue, the signal will be weaker due to either a large absorption for the emission wavelength or for the excitation wavelength, or both. This is clear in the melanin simulation where melanin has a larger absorption for lower wavelengths, which greatly penalizes the Nd:UCNPs for both excitation and emission wavelengths, reducing the gain obtained from the remainder of the volume. This has important practical consequences, as the skin contains melanin, and this effectively reduces the gain in the signal for these particles. However, for large amounts of lipid, both the excitation and emission wavelengths of the Nd:UCNPs are beneficial compared to the 975-nm excitation in the Yb:UCNPs. Thus, large amounts of lipid will cause the Nd:UCNPs to be beneficial over the Yb:UCNPs. Blood has a larger absorption at 650 nm compared to the other wavelengths, again causing a reduction in gain for large amounts of blood.

Another important aspect to bring forward is that the measurements and simulations were performed in transillumination.

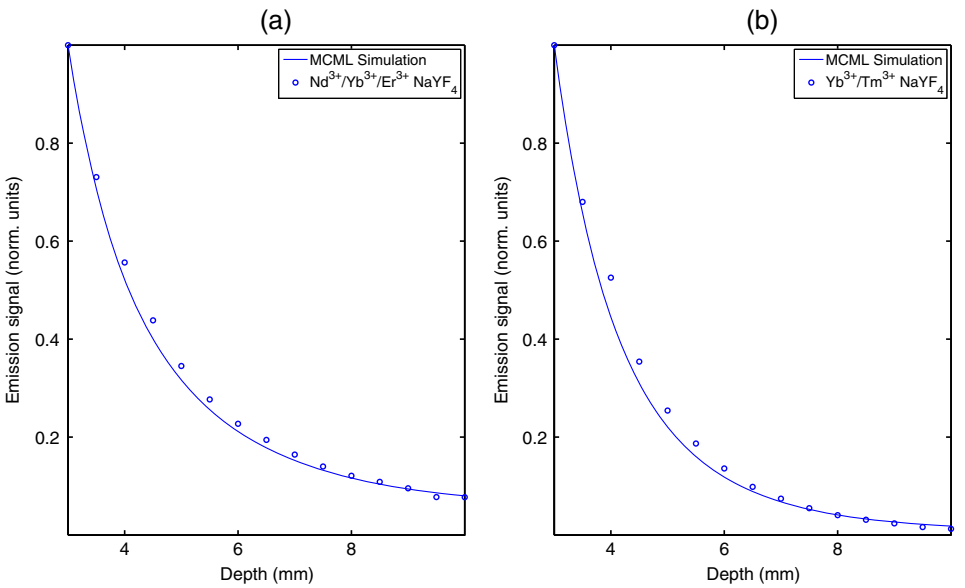

Fig. 5 Comparison of MCML simulation and experimental values: (a) $Nd^{3+}/Yb^{3+}/Er^{3+}$, and (b) Yb^{3+}/Tm^{3+}.

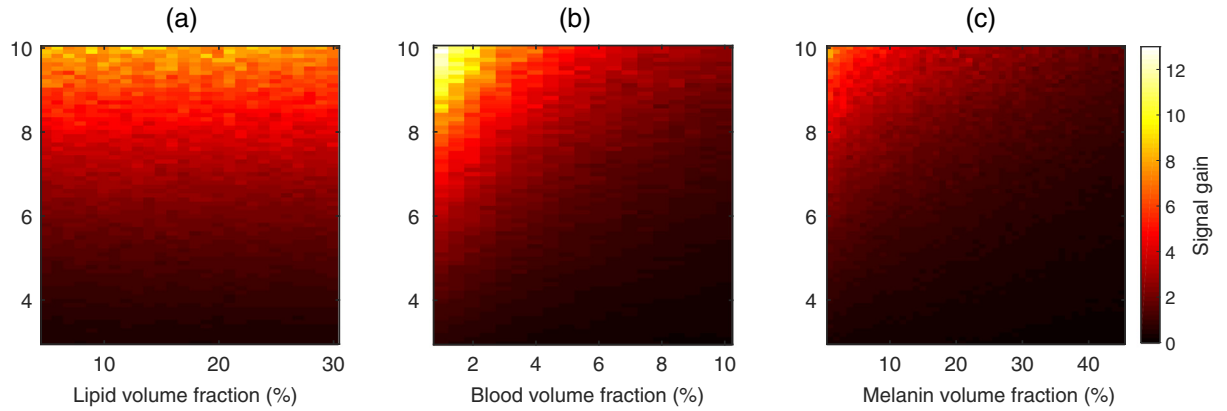

Fig. 6 MCML simulations with varying tissue compositions in an 18-mm thick tissue. The gain ratio of the signals for the Nd:UCNPs versus Yb:UCNPs is plotted as a function of tissue composition and sample depth inside the tissue: (a) simulates a varying lipid volume fraction from 5% to 30% with a step-size of 1%, (b) simulates a varying blood volume fraction from 1% to 10%, and (c) contains a 0.5-mm layer of skin including a melanin variation.

This means that for larger depths, the emission signal has a short path length. This is beneficial for the Nd:UCNPs in cases where the emission wavelength experiences a large absorption. It will at the same time penalize the signal for the same particles at lower depths, due to the much longer emission path length.

While there have been reports of other kinds of cosensitized upconversion using an organic dye as a cosensitizer in order to increase the spectral region of the absorption,[23] this report focuses on the Nd^{3+}/Yb^{3+} cosensitized UCNPs with an absorption peak at 808 nm. Any advantages for these particles in terms of improved signals for deep tissue regions should be directly transferable to dye–particles complexes.

The upconversion process in UCNPs is complex and differs depending on the rare-earth ions involved. It has been shown that a two-photon upconversion process will have a quadratic power dependence when not saturated.[24] Thus, the generated emission will depend quadratically on the fluence rate of the excitation light. A higher-excitation intensity will lead to saturation in some energy levels, causing the power dependence to gradually decrease from quadratic to linear.[24]

This study concerns deep tissue imaging, consequently at a very low excitation fluence rate, most likely far from any saturation effects. While comparing two kinds of UCNPs, it is necessary to confirm that they both are in the same region of saturation, in this case nonsaturated, to enable a generally valid comparison.

4 Conclusion

In conclusion, the Nd:UCNPs show a gain in signal at larger depths for most compositions of optical properties, mainly due to the reduced water absorption at 808 nm. The gain typically can be as high as 10 times for a depth of 10 mm. Melanin in the skin may to some extent reduce this gain in practical use. The gain suggests the Nd:UCNPs to be a promising substitution-for the Yb:UCNPs when performing deep tissue imaging in certain compositions of tissue.

Acknowledgments

The authors gratefully acknowledge Gökhan Dumlupinar for the help with the synthesis of the nanoparticles. This work was supported by a Swedish Research Council grant (VR).

References

1. C. T. Xu et al., "Autofluorescence insensitive imaging using upconverting nanocrystals in scattering media," *Appl. Phys. Lett.* **93**(17), 171103 (2008).
2. Q. Zhan et al., "Using 915 nm laser excited $Tm^{3+}/Er^{3+}/Ho^{3+}$-doped $NaYF_4$ upconversion nanoparticles for in vitro and deeper *in vivo* bioimaging without overheating irradiation," *ACS Nano* **5**(5), 3744–3757 (2011).
3. J.-H. Zeng et al., "Synthesis and upconversion luminescence of hexagonal-phase $NaYF_4$:Yb, Er^{3+} phosphors of controlled size and morphology," *Adv. Mater.* **17**(17), 2119–2123 (2005).
4. J.-C. Boyer et al., "Synthesis of colloidal upconverting $NaYF_4$ nanocrystals doped with Er^{3+}, Yb^{3+} and Tm^{3+}, Yb^{3+} via thermal decomposition of lanthanide trifluoroacetate precursors," *J. Am. Chem. Soc.* **128**(23), 7444–7445 (2006).
5. F. Wang and X. Liu, "Recent advances in the chemistry of lanthanide-doped upconversion nanocrystals," *Chem. Soc. Rev.* **38**(4), 976–989 (2009).
6. R. R. Anderson and J. A. Parrish, "The optics of human skin," *J. Invest. Dermatol.* **77**(1), 13–19 (1981).
7. G. M. Hale and M. R. Querry, "Optical constants of water in the 200-nm to 200-μm wavelength region," *Appl. Opt.* **12**(3), 555–563 (1973).
8. X. Xie et al., "Mechanistic investigation of photon upconversion in Nd^{3+}-sensitized core–shell nanoparticles," *J. Am. Chem. Soc.* **135**(34), 12608–12611 (2013).
9. F. Auzel, "Upconversion and anti-stokes processes with f and d ions in solids," *Chem. Rev.* **104**(1), 139–174 (2004).
10. Y.-F. Wang et al., "Nd^{3+}-sensitized upconversion nanophosphors: efficient in vivo bioimaging probes with minimized heating effect," *ACS Nano* **7**(8), 7200–7206 (2013).
11. W. M. Irvine and J. B. Pollack, "Infrared optical properties of water and ice spheres," *Icarus* **8**, 324–360 (1968).
12. Y. Zhao et al., "Optically investigating Nd^{3+}-Yb^{3+} cascade sensitized upconversion nanoparticles for high resolution, rapid scanning, deep and damage-free bio-imaging," *Biomed. Opt. Express* **6**, 838–848 (2015).
13. G. Chen et al., "Light upconverting core-shell nanostructures: nanophotonic control for emerging applications," *Chem. Soc. Rev.* **44**, 1680–1713 (2015).
14. G. Dumlupinar, "Crystal structure and luminescence studies of upconverting nanoparticles," Master's Thesis, Department of Physics, Lund University (2015).
15. B. Zhu et al., "Reduction of noise floor for molecular, fluorescence-enhanced optical imaging," *Proc. SPIE* **7891**, 789104 (2011).
16. B. Zhu et al., "Reduction of excitation light leakage to improve near-infrared fluorescence imaging for tissue surface and deep tissue imaging," *Med. Phys.* **37**(11), 5961–5970 (2010).
17. E. Alerstam et al., "Next-generation acceleration and code optimization for light transport in turbid media using GPUs," *Biomed. Opt. Express* **1**(2), 658–675 (2010).

18. S. Prahl, *Optical Absorption of Hemoglobin*, Oregon Medical Laser Center, Portland, OR (1999).
19. R. L. van Veen et al., "Determination of VIS-NIR absorption coefficients of mammalian fat, with time- and spatially resolved diffuse reflectance and transmission spectroscopy," presented at *Biomedical Topical Meeting, SF4* (2004).
20. S. L. Jacques et al., "Internal absorption coefficient and threshold for pulsed laser disruption of melanosomes isolated from retinal pigment epithelium," *Proc. SPIE* **2681**, 468–477 (1996).
21. B. Aernouts et al., "Supercontinuum laser based optical characterization of intralipid phantoms in the 500-2250 nm range," *Opt. Express* **21**(26), 32450–32467 (2013).
22. J. Swartling et al., "Accelerated Monte Carlo models to simulate fluorescence spectra from layered tissues," *J. Opt. Soc. Am. A* **20**(4), 714–727 (2003).
23. W. Zou et al., "Broadband dye-sensitized upconversion of near-infrared light," *Nat. Photonics* **6**(8), 560–564 (2012).
24. H. Liu et al., "Balancing power density based quantum yield characterization of upconverting nanoparticles for arbitrary excitation intensities," *Nanoscale* **5**(11), 4770–4775 (2013).

Biographies for the authors are not available.